Supporting Information

The effect of *in-situ* nitrogen doping on oxygen evolution reaction of MXenes

Yi Tang, Chenhui Yang, Yapeng Tian, Yangyang Luo, Xingtian Yin, and Wenxiu Que *

Electronic Materials Research Laboratory, Key Laboratory of the Ministry of Education & International Center for Dielectric Research, and Shaanxi Engineering Research Center of Advanced Energy Materials and Devices, School of Electronic & Information Engineering, Xi'an Jiaotong University, Xi'an 710049, Shaanxi, People's Republic of China.

*** Corresponding authors: wxque@mail.xjtu.edu.cn.**

Table of Contents

1. Experimental Section

1.1 Chemicals and Characterization

TiN (2-10 μm particle size, 99.50% purity, Aladdin), TiC (2-4 μm particle size, 99.00% purity, Aladdin), Al (1-3 μm particle size, 99.50% purity, Aladdin), Ti (≤ 48 μm particle size, 99.99% purity, Aladdin) and Nafion solution (5 wt% in deionized water) were purchased from Sigma-Aldrich. LiF (99.99 %), hydrochloric acid (technical grade) and KOH (99.99%) were purchased from Sinopharm Chemical Reagent Co., Ltd. Except as otherwise specified, all the chemicals were used without further purification. The high purity deionized water was purified using an UPH standard ultrapure water instrument (Sichuan ULUPURE pure science & technology Co., Ltd., China).

Scanning electron microscopy (SEM) images of the samples were observed using JSM-6390 with energy-dispersive X-ray analysis (EDAX) from JEOL Inc., Japan, and transmission electron microscopy (TEM) and selected area electron diffraction (SAED) results of the samples were obtained by using JEM-2010 from JEOL Inc., Japan. X-ray diffraction (XRD) patterns of the samples were performed on a Rigaku D/max 2200 pc diffractometer with Cu Kα radiation (λ = 0.15406 nm, 60 kV, 60 mA, 5° min^{-1} from 5 to 70°), and the XRD data were analyzed by using the Jade 6.0 software. Raman spectra measurements of the samples were performed by using a LabRam Aramis Raman spectrometer with a He-Ne laser (λ = 633 nm). The electronic state and composition of the samples were recorded by an X-ray photoelectron spectrometer (XPS, ESCALAB Xi+, Thermo Fisher Scientific, USA) with an exciting source of Al Kα (400 W, 45 eV pass energy, 650 μm spot size). Contact angles of the films were measured by using the contact angle measurement instrument JC2000D2 (POWEREACH, Shanghai zhongchen Digital Technology Apparatus Co., Ltd., China). The thickness of the film was measured by using a high-accuracy submicrometer digimatic micrometer (293-240, Mitutoyo, Japan) with a resolution of 1 μm. For electric conductivity test, the current and the potential of the test device were measured by using a Linear Sweep Voltammetry (LSV) method in a CHI 660E electrochemical workstation.

1.2 Synthesis of the Ti_3AlC_2, $Ti_3AlC_{1.8}N_{0.2}$ and $Ti_3AlC_{1.6}N_{0.4}$ ceramic powders

Firstly, all powders of TiC (2-4 μm particle size, 99.00% purity, Aladdin), Al (1-3 μm particle size, 99.50% purity, Aladdin) and Ti (≤ 48 μm particle size, 99.99% purity, Aladdin) were mixed in a molar ratio of 2:1.2:1. The mixed powders were ball-milled with ethyl alcohol for 6 h at a speed of 400 rpm, and dried in a vacuum oven at 40 °C for 24 h. Then, the dried mixture was annealed in an alundum tube

in Ar gas at a flow of 40 mL min^{-1}. The sintering process was conducted at 1350 °C for 2 h at a heating rate of 8 ^{o}C min^{-1}. The sintered product was grinded by stainless steel mortar and sieved through a 400 mesh screen for the sake of the initial particle size was controlled at < 38 μm. Thus, the Ti_3AlC_2 powders were obtained for further study.

The synthesis processes of the $Ti_3AlC_{1.8}N_{0.2}$ and $Ti_3AlC_{1.6}N_{0.4}$ powders were similar to that of the Ti_3AlC_2 powders except for the molar ratios of mixed powders were adjusted to TiN:TiC:Al:Ti = 0.2:1.8:1.2:1 for the $Ti_3AlC_{1.8}N_{0.2}$ powders and TiN:TiC:Al:Ti = 0.4:1.6:1.2:1 for the $Ti_3AlC_{1.6}N_{0.4}$ powders, respectively.

1.3 Synthesis of the few-layered Ti_3C_2, $Ti_3C_{1.8}N_{0.2}$ and $Ti_3C_{1.6}N_{0.4}$ flakes

As shown in the Figure S1, the few-layered $Ti_3C_{1.6}N_{0.4}$ flakes were prepared according to the precious work with a certain modification [1]. Firstly, slowly adding 2 g LiF powders to 20 mL 9 M HCl aqueous solution with stirring for 30 min to achieve the mixed etching solution. Then, 1 g of the as-prepared $Ti_3AlC_{1.6}N_{0.4}$ powders were slowly added to the above mixed etching solution, then stirred at a speed of 200 rpm at 35 °C for 24 h. Afterward, the solid residue was repeatedly washed with ultrapure water until the pH value of the supernatant was larger than 6. Then, the $Ti_3C_{1.6}N_{0.4}$ sediments were dispersed in 200 mL of de-oxygenated ultrapure water and sonicated for 60 min under Ar flow in ice-bath. Finally, the dark green supernatant was collected by centrifuging for 30 min at 1500 rpm, and named as few-layered $Ti_3C_{1.6}N_{0.4}$ suspension. The $Ti_3C_{1.6}N_{0.4}$ suspension was restored at 4 °C in the refrigerator before being used. The synthesis processes of the $Ti_3C_{1.8}N_{0.2}$ flakes and Ti_3C_2 flakes were similar to that of the $Ti_3C_{1.6}N_{0.4}$ flakes.

1.4 Electrode preparation and electrochemical testing

Active materials (4.0 mg, e.g. Ti_3C_2 flakes, $Ti_3C_{1.8}N_{0.2}$ flakes or $Ti_3C_{1.6}N_{0.4}$ flakes) was mixed with ethanol (500 μL), ultrapure water (485 μL) and Nafion (15 μL, 5.0 wt%), followed in ice-bath ultrasonication for 40 min to form a uniform suspension. The electrocatalyst ink (12.5 μL) was then loaded onto a pretreated piece of carbon fiber paper (CFP, 0.25 cm × 0.25 cm) and dried under ambient condition for 6 h. The average mass loading was calculated to be around 0.2 mg cm^{-2}.

The performance of the electrocatalysts towards OER was executed on a CHI 660E electrochemical workstation (CH Instruments, China) under room temperature with a standard three-electrode system, including a working electrode (Ti_3C_2 flakes, $Ti_3C_{1.8}N_{0.2}$ flakes or $Ti_3C_{1.6}N_{0.4}$ flakes), a counter electrode

(Pt foil, area of 1.0 cm × 1.0 cm) and a reference electrode (SCE). Before the measurements, the aqueous electrolyte of 1 M KOH was bubbled with N_2 flow (30 mL min^{-1}) for 30 min. During measuring, a slow gas flow (5 mL min^{-1}) should be maintained over the electrolyte to ensure continuous gas saturation. The linear sweep voltammetry (LSV) was obtained at a low scan rate of 5 mV s^{-1}. The electrical double-layer capacitance (Cdl) of the electrocatalyst was measured from cyclic voltammetry (CV) in a small potential range of 1.17 – 1.27 V *vs*. RHE without apparent faradic processes occurring. The plot of the current density difference [$\Delta j = (j_a - j_c)/2$] at 1.22 V *vs*. SCE against the scan rates (10 – 100 mV s^{-1}) was linearly fitted, and its slope was the C_{dl} of the tested electrocatalysts. Electrochemical impedance spectroscopy (EIS) measurement was conducted at a potential of 1.62 V *vs*. RHE by applying an AC voltage with amplitude of 5 mV in a frequency range from 100 kHz to 10 mHz. Chronopotentiometric measurement was carried out through applying a current density of 10 mA cm^{-2} for 12 h.

2. Calculation

All measured potentials *vs*. SCE are converted to a reversible hydrogen electrode (RHE) potential based on the Nernst equation as below:

$$E\ vs.\ RHE\ (V) = E\ vs.\ SCE\ (V) + 0.05916 \times \mathrm{pH} + 0.2412\ (\mathrm{V}) \quad (1)$$

where *E vs. RHE* is the applied potential *vs*. RHE; *E vs. SCE* is the applied potential *vs*. SCE reference electrode, pH is the pH value of the electrolyte (1 M KOH, pH=14).

The overpotential is calculated according to the following formula (2):

$$\eta\ (\mathrm{V}) = \mathrm{E}\ vs.\ \mathrm{RHE} - 1.23\ (\mathrm{V}) \quad (2)$$

Tafel slope is calculated by plotting overpotential η *vs.* logarithm of current density from polarization curves according to the following equation.

$$\eta\ (\mathrm{V}) = b \times \log j \quad (3)$$

where η is the overpotential, b is the Tafel slope, j is the current density.

The calculation of ECSA is based on the measured double-layer capacitance (C_{dl}) of the synthesized electrode. The C_{dl} of the electrocatalyst is measured from CV curves in a small potential range of 1.17 – 1.27 V without apparent faradaic processes occurring. The plot of the current density difference at 1.22 V against the scan rates (10 − 100 mV s^{-1}) is linearly fitted, and its slope is the twice C_{dl} of the tested electrocatalyst.

For the electric conductivity test, as shown in Figure S5, the current and the potential of the test device are measured by using a Linear Sweep Voltammetry (LSV) method in a CHI 660E electrochemical workstation.

The conductivity κ (S cm^{-1}) of the $Ti_3C_{1.6}N_{0.4}$ film can be calculated according to the following equations:

$$R = U / I \quad (4)$$

$$\rho = R\ S / L \quad (5)$$

$$\kappa = 1 / \rho = L / (R \times S) \quad (6)$$

$$\kappa = (I \times L) / (U \times S) \quad (7)$$

where κ (S cm^{-1}) is electrical conductivity, ρ (Ω·cm) is the resistivity, and R (Ω) is resistance. I (A) is the response current between the $Ti_3C_{1.6}N_{0.4}$ films (remove the current of other components), L (cm) is the thickness of the film, U (V) is the potential, S (cm^2) is the effective contact area between the film and GCE.

3. Figures

Figure S1.

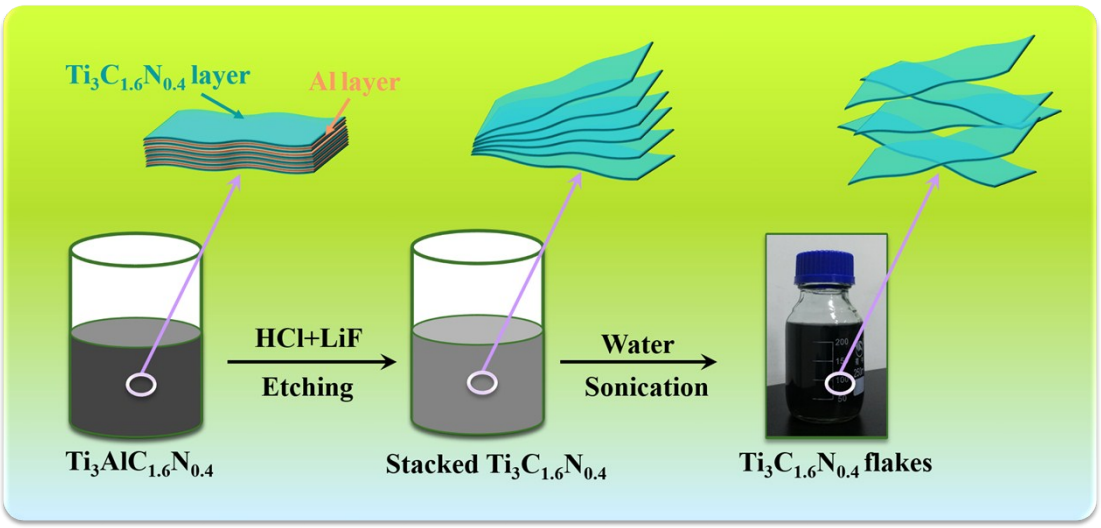

Figure S1. Schematic preparation procedure of the $Ti_3C_{1.6}N_{0.4}$ flakes.

Figure S2.

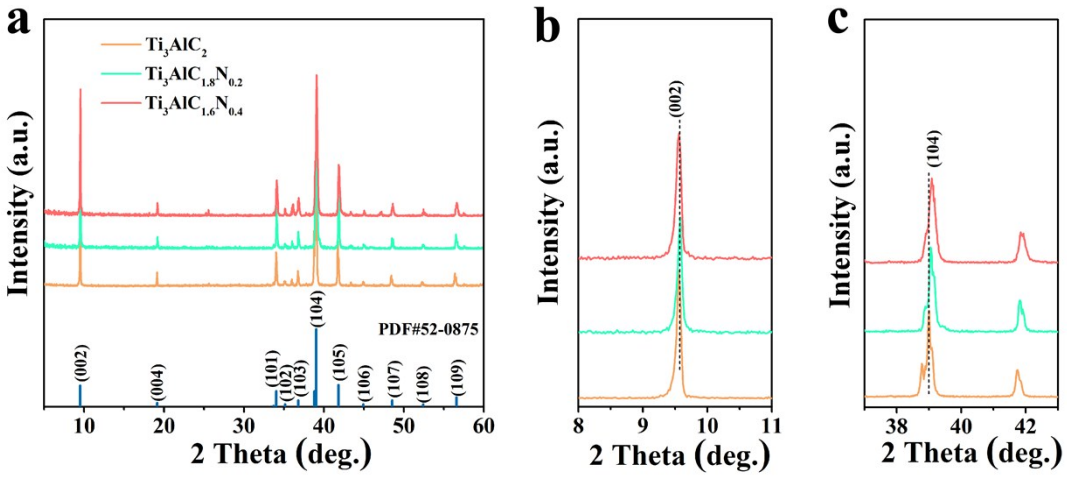

Figure S2. (a) XRD patterns, the corresponding diffraction peaks at around (b) (002) and (c) (104) of the Ti_3AlC_2, $Ti_3AlC_{1.8}N_{0.2}$ and $Ti_3AlC_{1.6}N_{0.4}$ powders.

Figure S3.

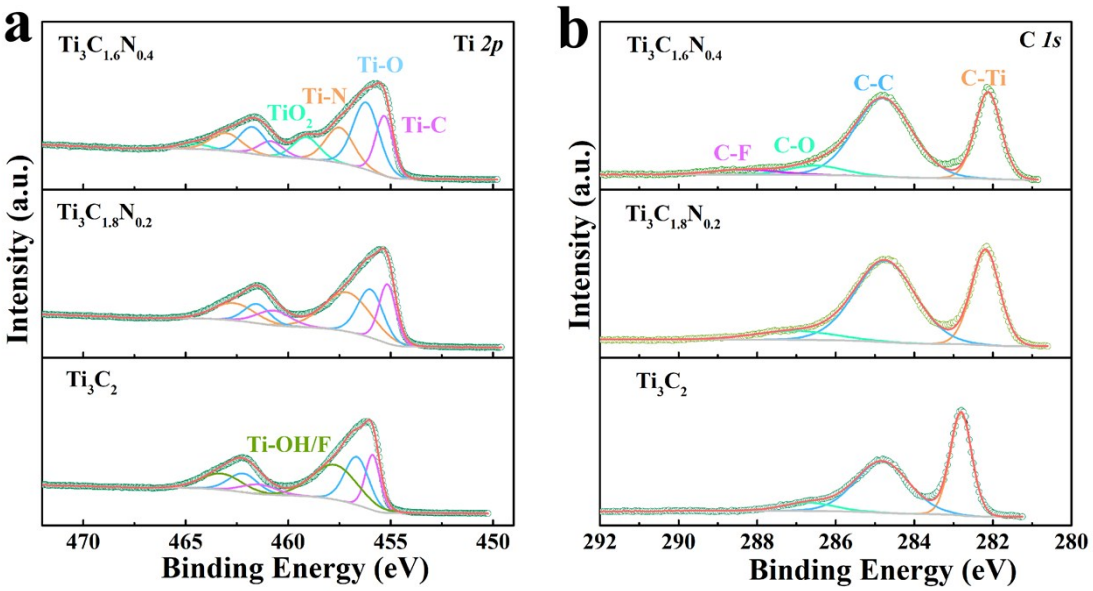

Figure S3. (a) Ti *2p* spectra and (b) C *1s* spectra of the Ti_3C_2, $Ti_3C_{1.8}N_{0.2}$ and $Ti_3C_{1.6}N_{0.4}$ samples.

Figure S4.

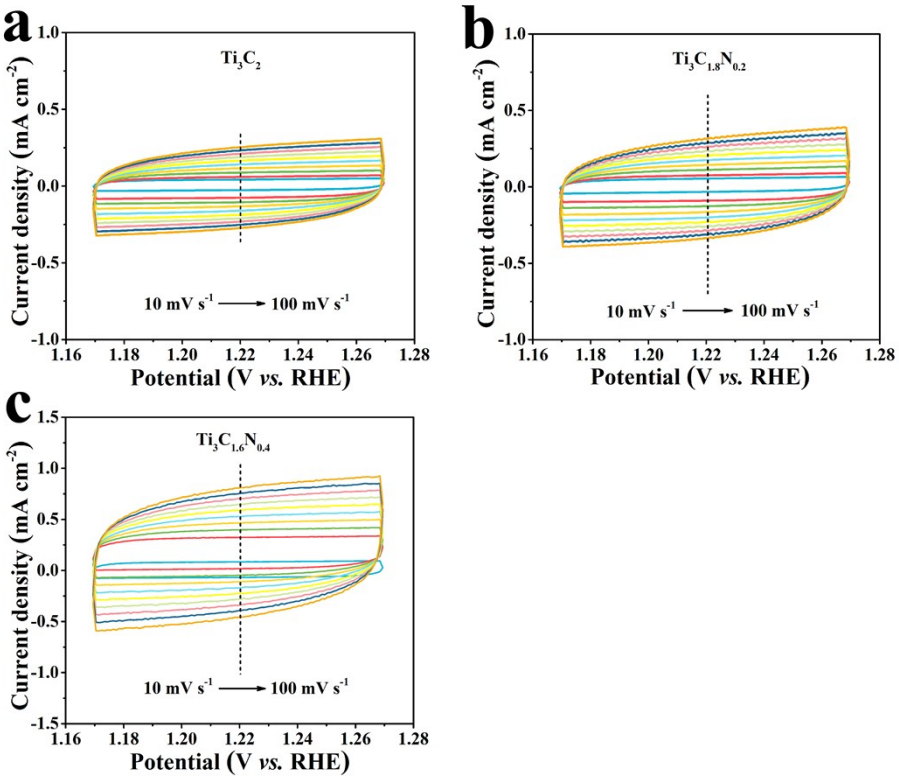

Figure S4. CV curves of the Ti_3C_2 (a), $Ti_3C_{1.8}N_{0.2}$ (b), and $Ti_3C_{1.6}N_{0.4}$ (c) electrocatalysts at various scan rates.

Figure S5.

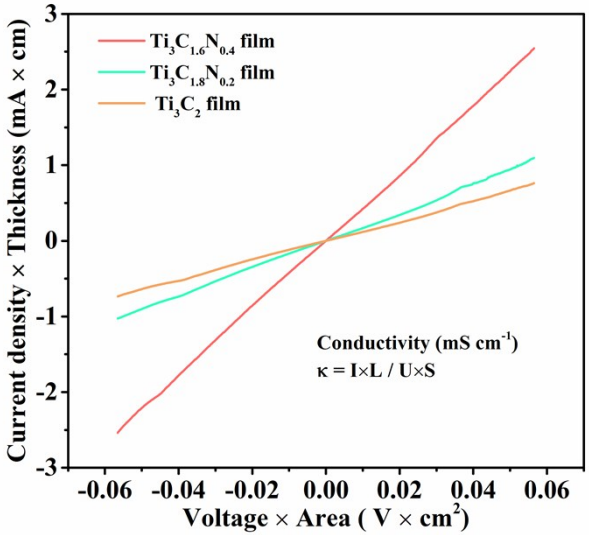

Figure S5. Curves of conductivity of the Ti_3C_2, $Ti_3C_{1.8}N_{0.2}$ and $Ti_3C_{1.6}N_{0.4}$ electrocatalysts.

Figure S6.

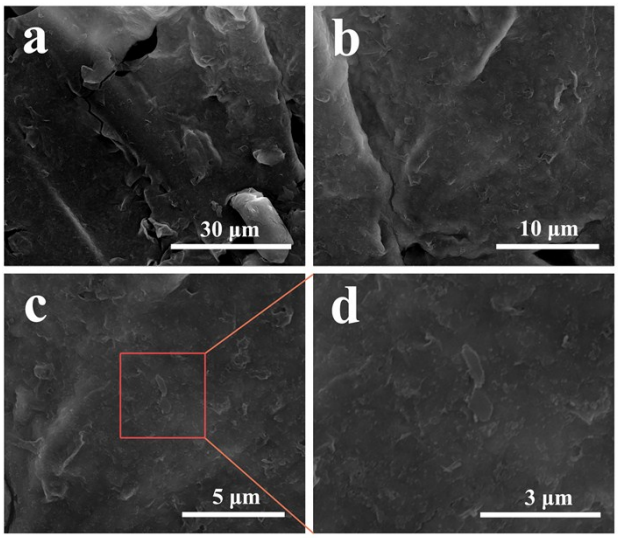

Figure S6. The SEM images of the $Ti_3C_{1.6}N_{0.4}$ catalysts after cycling at current density of 10 mA cm^{-2} for 12 h.

4. Tables

Table S1. XPS results of the Ti_3C_2, $Ti_3C_{1.8}N_{0.2}$ and $Ti_3C_{1.6}N_{0.4}$ samples.

Sample	Ti *2p* (at.%)	C *1s* (at.%)	N *1s* (at.%)	O *1s* (at.%)	F *1s* (at.%)	Cl *2p* (at.%)
Ti_3C_2	26.26	44.62	-	12.01	12.15	4.95
$Ti_3C_{1.8}N_{0.2}$	24.07	45.39	3.76	13.63	8.72	4.43
$Ti_3C_{1.6}N_{0.4}$	21.47	44.17	5.72	15.70	9.16	3.79

Table S2. XPS results of the contents of different nitrogen species in the $Ti_3C_{1.8}N_{0.2}$ and $Ti_3C_{1.6}N_{0.4}$ electrocatalysts.

Catalysts	N-Ti (at.%)	N-5 (at.%)	N-Q (at.%)	N-6 (at.%)
$Ti_3C_{1.8}N_{0.2}$	52.46	41.20	6.33	-
$Ti_3C_{1.6}N_{0.4}$	61.75	21.85	13.52	2.88

Table S3. Simulated R_s and R_{ct} and CPE values of the Ti_3C_2, $Ti_3C_{1.8}N_{0.2}$ and $Ti_3C_{1.6}N_{0.4}$ electrocatalysts.

Catalysts	R_s (ohm)	R_{ct} (ohm)	CPE-T (ohm)	CPE-P (ohm)
Ti_3C_2	5.39	2692	0.00107	0.86828
$Ti_3C_{1.8}N_{0.2}$	4.88	2113	0.0014	0.86554
$Ti_3C_{1.6}N_{0.4}$	3.12	279.2	0.0031	0.96554

References

1. Y. Tang, C. Yang, Y. Yang, X. Yin, W. Que and J. Zhu, *Electrochim. Acta*, 2019, **296**, 762-770.